Chemical Science

ROYAL SOCIETY OF CHEMISTRY

EDGE ARTICLE

View Article Online
View Journal | View Issue

Cite this: *Chem. Sci.*, 2023, **14**, 8524

All publication charges for this article have been paid for by the Royal Society of Chemistry

Received 5th May 2023
Accepted 11th July 2023

DOI: 10.1039/d3sc02292g

rsc.li/chemical-science

A dinuclear Rh(−I)/Rh(I) complex bridged by biphilic phosphinine ligands†

Koichiro Masada, Kiyosumi Okabe, Shuhei Kusumoto and Kyoko Nozaki *

Bimetallic complexes have enabled precise control of catalysis by accumulating two discrete metal centres. In these complexes, bridging ligands are essential to combine multiple metals into one molecule. Among some bridging modes, an unsymmetric bridging mode will differentiate the electronic structures of the two metal centres. In this study, a dinuclear Rh(−I)/Rh(I) complex bridged by tridentate phosphine–phosphinine–phosphine ligands was prepared by reduction of the corresponding Rh(I) complex. Single-crystal X-ray analysis and DFT calculations suggest that the phosphinine ligands adopt an unsymmetric bridging mode wherein phosphinine accepts d-electrons from one Rh centre and, at the same time, donates lone pairs to the other Rh centre.

Introduction

Combining multiple metals is an attractive method to accumulate more than one function in one complex enabling precise tuning of the reactivity of each metal centre.[1–5] Bridging ligands play a crucial role in constructing a rigid multimetallic skeleton and facilitating electronic communication between metals. The coordination mode of bridging ligands can be classified into the following three types (Fig. 1a). Two electron donors, such as a hydride anion and carbanions, form three-centre two-electron bonding (Type I).[6] Anionic ligands with lone pairs, such as halide or dianionic ligands, can donate four electrons *via* two σ bonds with each metal centre (Type II).[6] When a ligand simultaneously has a lone pair and an electron-accepting orbital, the bridging ligand enables an unsymmetric coordination environment where two electrons are donated from a ligand to an electron-poor metal, and two electrons are accepted from an electron-rich metal (Type III). For example, the carbonyl ligand (CO) bridges two or more metal centres, and it has some bridging modes (Fig. 1b);[7] Type I with a lone pair on the C atom, Type II where CO donates four electrons by both σ- and π-donation,[8] and Type III where the carbon atom coordinates to one metal centre with a σ-type lone pair and accepts two electrons from the other metal centre using the π*-orbital. Since a Type III bridging mode was found in a dinuclear iron carbonyl complex in 1961,[9] this bridging mode has been observed in some dinuclear metal carbonyl complexes.[10–12]

Phosphinine (phosphabenzene) is a well-studied equivalent to carbon monoxide in organometallic chemistry since phosphinine exhibits σ-donating and strong π-accepting properties due to its low-lying π* orbital on the P atom.[13–15] To date, numerous phosphinine metal complexes have been synthesized, exhibiting various coordination modes, reactivities, and physical properties, derived from the π-acidity of phosphinine ligands.[15–18] Thanks to their strong π-accepting properties, phosphinine ligands often show biphilic reactivity, such as nucleophilic attacks at the P atom[19,20] and metal–ligand cooperative C=O bond cleavage of CO_2.[21] Phosphinine compounds form multinuclear complexes by the bridging of the P atom like the carbonyl ligand while the use of multidentate ligands also afforded multinuclear complexes.[22–26] Phosphinine can exhibit all three bridging modes illustrated in Fig. 1c;[27] Type I with a lone pair on the phosphorus atom,[28–34] Type II with

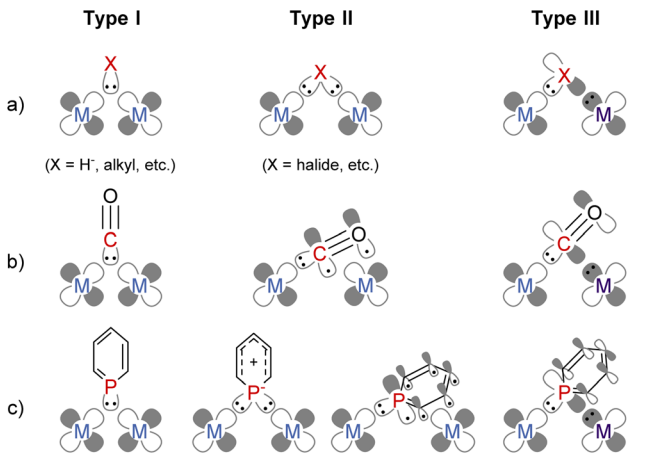

Fig. 1 Classification of the electronic structures of bridging ligands; (a) general description; (b) carbonyl ligands; (c) phosphinine ligands.

Department of Chemistry and Biotechnology, Graduate School of Engineering, The University of Tokyo, 7-3-1 Hongo, Bunkyo-ku, Tokyo 113-8656, Japan. E-mail: nozaki@chembio.t.u-tokyo.ac.jp

† Electronic supplementary information (ESI) available. CCDC 2260653 and 2260654. For ESI and crystallographic data in CIF or other electronic format see DOI: https://doi.org/10.1039/d3sc02292g

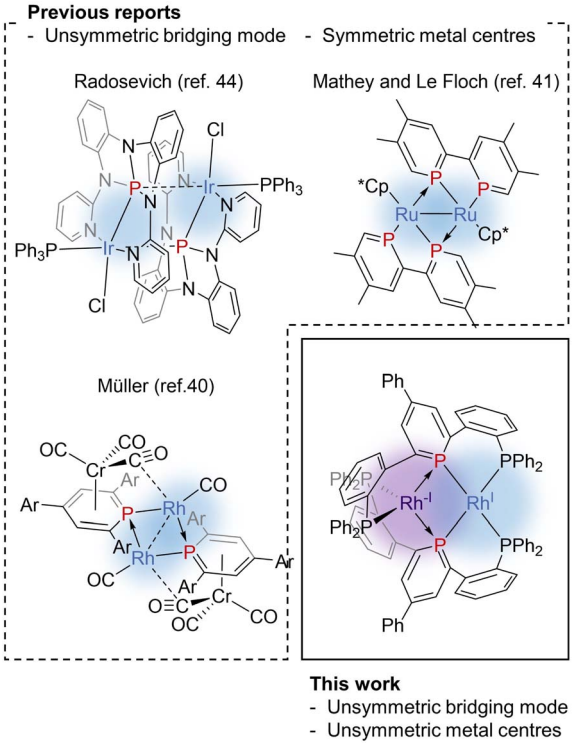

Fig. 2 Previous reports on unsymmetrically bridging phosphorus ligands and this work, a Rh(−I)/Rh(I) dinuclear complex bridged by phosphinine pincer ligands.

a phosphide-like resonance structure[28,35–37] or 8e donor character where both the lone pair on the P atom and π-electrons of the phosphinine ring are donated,[38–40] and Type III utilizing the lone pair and the low-lying π* orbital.[40,41] Mathey, Le Floch, and co-workers reported that a dinuclear ruthenium complex with bisphosphinine ligands showed Type III bridging mode (Fig. 2).[41] Recently, Müller and co-workers reported that an η^6-phosphinine chromium complex acted as a Type III bridging ligand to form dirhodium complexes (Fig. 2).[40] Geometrically constrained tricoordinate phosphorus compounds are another class of biphilic phosphorus compounds.[42] They exhibited phosphorus-centred bond activation reactions and related catalytic activities, although their coordination chemistry is less explored than that of phosphinine ligands. Radosevich and co-workers reported that geometrically constrained tricoordinate phosphorus ligands show electrophilic reactivity[43] and form an iridium dinuclear complex in a Type III manner (Fig. 2).[44] Although the acid/base bifunctional character is quite beneficial to construct an unsymmetric multimetallic environment, to the best of our knowledge, there is no example where a phosphinine ligand is employed to bridge two metal centres in different electronic states.

Recently, we reported a phosphinine pincer ligand bearing two phosphine pendants.[45] The phosphine ligands stabilize the coordination of the phosphinine moiety. The phosphinine ligand formed a dinuclear complex when coordinated to silver centres.[46] Here, in this report, we present syntheses and structural analysis of a dinuclear Rh(−I)/Rh(I) complex bridged by phosphinine pincer ligands (Fig. 2). Unlike the precedents shown in Fig. 2, the two rhodium centres are non-equivalent, where one rhodium centre can be regarded as a two electron-accepting Rh(I) centre, and the other can be regarded as a two electron-donating Rh(−I) centre.

Results and discussion

The pincer ligand **1** was synthesized following our previous report.[46] By treating ligand **1** with $[RhCl(cod)]_2$, an orange powder was obtained. The powder was insoluble in common solvents, which suggests that a bimetallic or polymetallic structure was formed in the solid. The product was reduced by sodium naphthalenide to afford dinuclear Rh complex **2** in 43% yield (Scheme 1). The structure of complex **2** was determined by single-crystal X-ray crystallographic analysis (Fig. 3). Further reduction to dinuclear Rh(−I)/Rh(−I) complex **3** was observed in the reaction by using an excess amount of metallic sodium (see the ESI† for details). The structure of **3** was determined by X-ray crystallography (Fig. 4) although **3** was too unstable to be fully characterized by spectroscopic methods.

Complex **2** has an unsymmetric structure where both phosphinine rings tilt to one Rh centre (∠C3–P1–P4 = 160.9° and ∠C50–P4–P1 = 165.0°). One Rh centre (Rh1) adopts tetrahedral geometry (τ_4 = 0.83), whereas the other Rh centre (Rh2) adopts distorted square planar geometry (τ_4 = 0.39)[47] (*vide infra* for detailed discussions on the unsymmetric structure of complex **2**). Complex **3** also has an unsymmetric structure where one phosphinine ring tilts to one Rh centre (∠C50–P4–P1 = 156.9°) and the other phosphinine ring shows symmetric coordination (∠C3–P1–P4 = 178.0°). In complex **3**, both Rh centres adopt tetrahedral geometry (τ_4 = 0.67 and 0.78). DFT calculations (calculated at the PBE0-D3/def2-SVP level) suggest that the unsymmetric coordination of phosphinine is due to the perturbation by the contact of the Na cations. The calculated structure of complex **3** matched with the experimental result (Fig. S10†). When the geometry optimization of complex **3** was conducted without the contacting Na cations, the resulting structure showed symmetric coordination of both phosphinine rings (Fig. S11†). These results suggest that the unsymmetric coordination in complex **3** is mainly derived from the contacting Na cations.

The geometries of complex **2** can be rationalized as follows. The distorted square planar geometry of Rh2 suggests that it

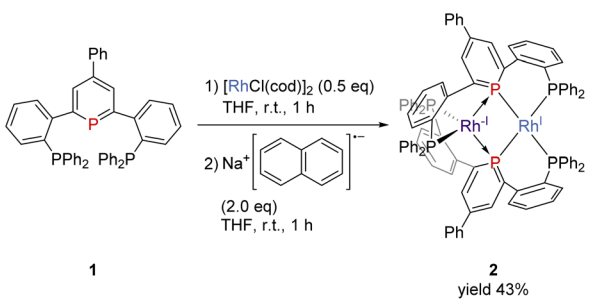

Scheme 1 Formation of complex **2**.

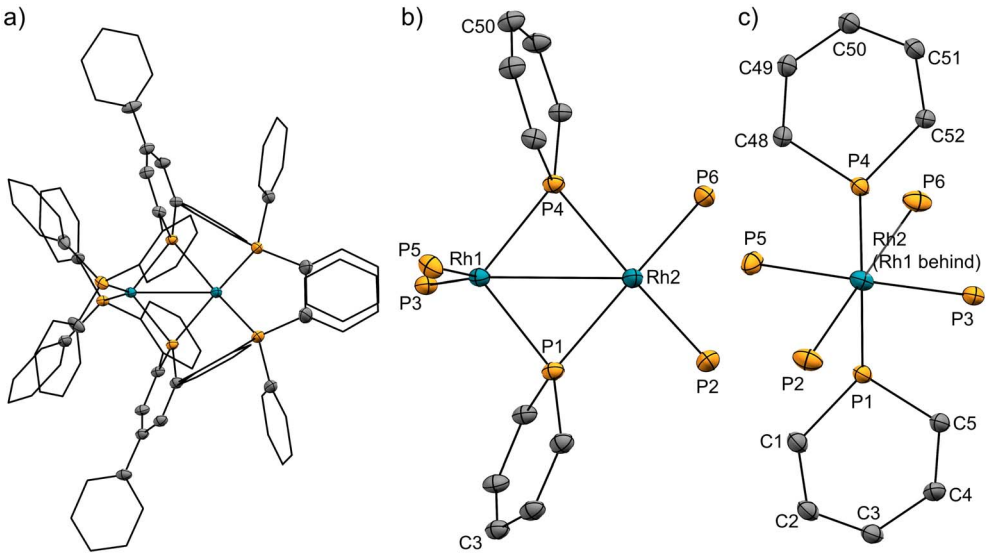

Fig. 3 (a) X-ray crystal structure of complex **2** (thermal ellipsoids are drawn with 50% probability; the hydrogen atoms are omitted, and the phenyl groups and the phenylene linkers are simplified for clarity); (b) and (c) geometries around rhodium and phosphorus atoms. Selected bond lengths [Å] and bond angles [deg]: Rh1⋯Rh2, 2.8493(3); Rh1–P1, 2.2262(8); Rh1–P4, 2.2182(8); Rh1–P3, 2.2848(8); Rh1–P5, 2.2840(8); Rh2–P1, 2.2731(8); Rh2–P4, 2.2884(8); Rh2–P2, 2.2554(9); Rh2–P6, 2.2569(9); P1–C1, 1.758(3); P1–C5, 1.763(3); C1–C2, 1.387(5); C2–C3, 1.411(5); C3–C4, 1.408(4); C4–C5, 1.384(4); P4–C48, 1.767(3); P4–C52, 1.758(3); C48–C49, 1.377(4); C49–C50, 1.399(4); C50–C51, 1.408(4); C51–C52, 1.392(4); P1–Rh1–P5, 112.40(3); P3–Rh1–P5, 130.89(3); P1–Rh2–P6, 152.26(3); P2–Rh2–P4, 152.65(3).

has Rh(I) character. The unsymmetric coordination mode of the phosphinine ligands suggests that the phosphinine ligands behave as Z-type ligands on the Rh1 centre. In comparison with the computed structure of a model ML_2Z_2-type Rh(−I) complex, $[Rh(PMe_3)_2(BMe_3)_2]^-$ (Fig. S12†), the geometry around Rh1 is consistent with Rh(−I) character. The P–Rh–P angles ($\angle$P3–Rh1–P5 = 130.9° for complex **2** and $\angle$P–Rh–P = 138.6° for $[Rh(PMe_3)_2(BMe_3)_2]^-$) and the geometry indices (τ_4 = 0.83 for Rh1 in complex **2**, τ_4 = 0.76 for $[Rh(PMe_3)_2(BMe_3)_2]^-$) resemble each other (see the ESI† for further discussion). Consequently,

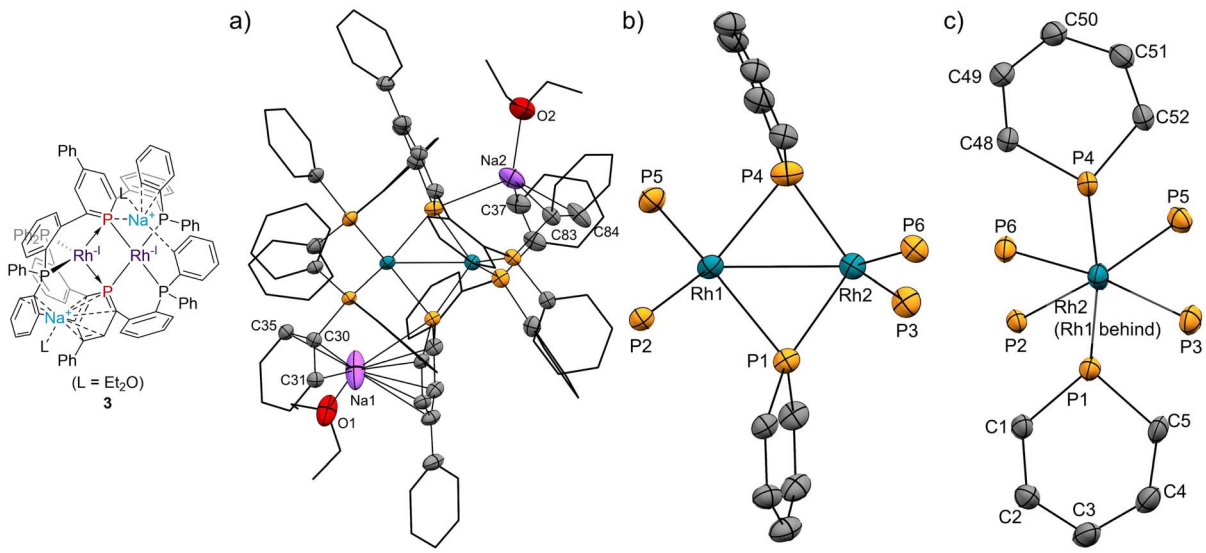

Fig. 4 (a) X-ray crystal structure of complex **3** (thermal ellipsoids are drawn with 50% probability; the hydrogen atoms are omitted, and the phenyl groups and the phenylene linkers are simplified for clarity); (b) and (c) geometries around rhodium and phosphorus atoms. Selected bond lengths [Å] and bond angles [deg]: Rh1⋯Rh2, 2.7436(4); Rh1–P1, 2.3335(10); Rh1–P4, 2.3666(11); Rh1–P2, 2.2375(10); Rh1–P5, 2.2785(10); Rh2–P1, 2.2278(10); Rh2–P4, 2.2275(11); Rh2–P3, 2.2575(11); Rh2–P6, 2.2440(10); P1–C1, 1.802(4); P1–C5, 1.804(4); C1–C2, 1.377(5); C2–C3, 1.426(6); C3–C4, 1.403(6); C4–C5, 1.384(6); P4–C48, 1.799(4); P4–C52, 1.793(4); C48–C49, 1.372(6); C49–C50, 1.409(6); C50–C51, 1.391(6); C51–C52, 1.398(5); P1–Na1, 3.149(3); Na1–C1, 2.993(5); Na1–C2, 2.947(5); Na1–C3, 2.911(5); Na1–C4, 2.731(5); Na1–C5, 2.708(5); Na1–C30, 2.732; Na1–C31, 3.015(5); Na1–C35, 2.793(5); P4–Na2, 2.976(3); Na2–C37, 2.848(6); Na2–C83, 2.987(5); Na2–C84, 2.818(8); P1–Rh1–P4, 101.59(4); P2–Rh1–P5, 113.64(4); P1–Rh2–P4, 109.67(4); P3–Rh2–P6, 119.85(4).

the electronic structure of complex **2** is an unsymmetric Rh(−I)/Rh(I) dinuclear structure, as shown in Scheme 1. This description is also supported by the bond lengths between Rh centres and phosphorus atoms. Rh1 had shorter distances from the P atoms on the phosphinine rings (Rh1–P1 = 2.2262 Å and Rh1–P4 = 2.2182 Å) than Rh2 (Rh2–P1 = 2.2731 Å and Rh2–P4 = 2.2884 Å) whereas Rh1 had longer distances from P atoms on the phosphine moiety (Rh1–P3 = 2.2848 Å and Rh1–P5 = 2.2840 Å) than Rh2 (Rh2–P2 = 2.2554 Å and Rh2–P6 = 2.2569 Å). Phosphinine ligands act as a strong π-acceptor and weak σ-donor, so P atoms on the phosphinine rings have stronger interaction with the Rh(−I) centre, which acts as a strong electron-donor.

In addition, the X-ray photoelectron spectroscopy (XPS) analysis of complex **2** was conducted to obtain more information on the electronic states of the Rh centres (Fig. 5). The XPS spectrum showed that complex **2** contains both Rh(I) species (311.7 and 307.0 eV) and Rh(−I) species (310.8 and 306.1 eV). For the binding energy of Rh $3d_{5/2}$, the higher value (307.0 eV) is slightly lower than that of referential Rh(I) species ($[RhCl(C_2H_4)_2]_2$: 307.3 eV; $RhCl(PPh_3)_3$: 307.4 eV).[48] The lower value (306.1 eV) is lower than that of metallic Rh (307.0 eV)[49] and a reported Rh(−I) species, $[K(18\text{-crown-6})][Rh(CO)(PPh_3)_3]$[50] (306.8 eV, see Fig. S8† for the XPS spectrum measured in this work). These results strongly support that the Rh centres in complex **2** have unsymmetric Rh(−I)/Rh(I) character.

The ^{31}P NMR spectrum of complex **2** (Fig. 6) showed two peaks with complex coupling patterns by J_{PP} and J_{PRh}, which accords with the dinuclear structure observed in the solid state. The ^{1}H, ^{13}C, and ^{31}P NMR spectra suggest that all the PPh_2 moieties are chemically equivalent, possibly due to the flipping of the phosphinine rings that is faster than the timescale of NMR (*vide infra* for the calculation of the stability of the unsymmetric structure). Under more concentrated conditions, ^{31}P NMR showed complicated NMR spectra, probably due to aggregation (see Fig. S6 in the ESI† for details).

DFT calculations were employed to obtain deeper insight into the electron donation from the Rh(−I) centre to the phosphinine ring in complex **2**. The calculation in the gas phase reproduced the unsymmetric structure of complex **2**, which was observed in the solid state. In addition, a symmetric structure could not be located as a stable intermediate but exists as a transition state of the flipping of the phosphinine rings (Fig. 7). The activation energy is 9.0 kcal mol^{-1} (calculated at the ωB97XD/def2-TZVP//PBE0-D3/def2-SVP level), which supports the discussion that fast flipping of the phosphinine rings

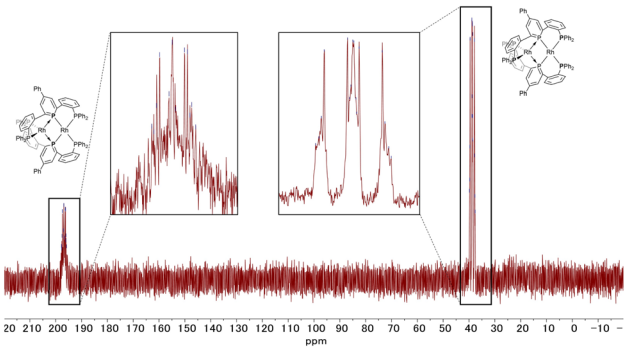

Fig. 6 ^{31}P NMR spectrum of complex **2** (202 MHz, THF-d_8).

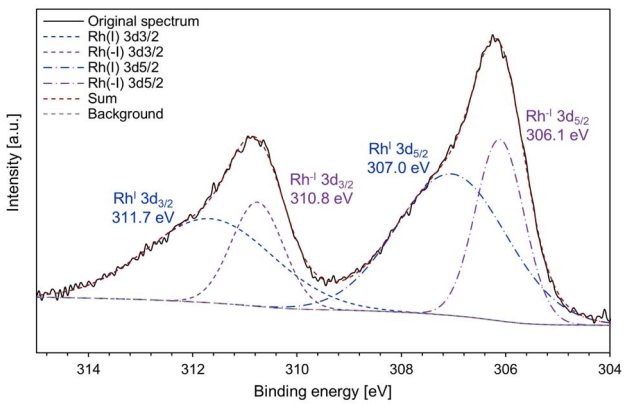

Fig. 5 The XPS spectrum of complex **2**. The continuous black line indicates the original spectrum; the blue and purple dashed lines indicate the deconvoluted signals; the red dashed line is the sum of the deconvoluted signals; the grey dashed line is the background signal.

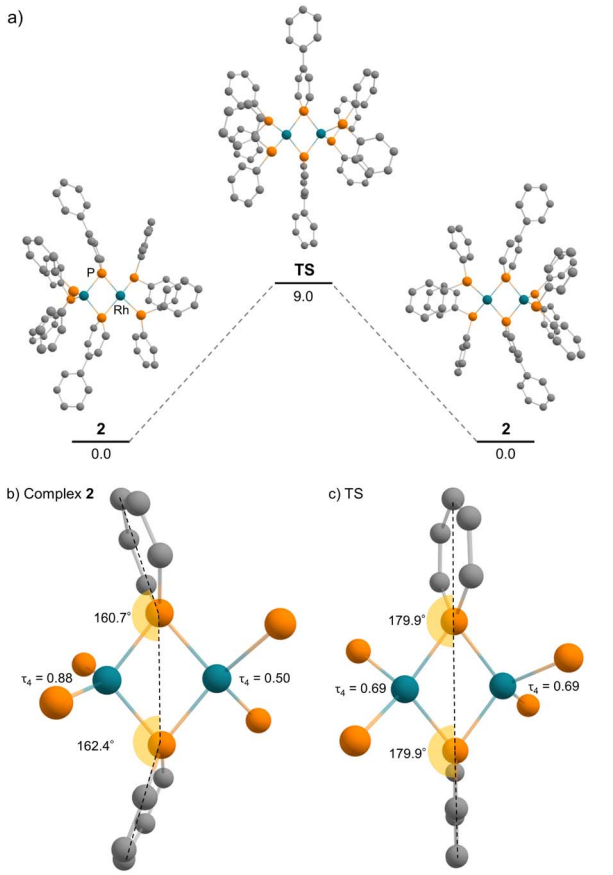

Fig. 7 (a) Energy diagram of the flipping of the phosphinine rings (unit: kcal mol^{-1}); (b) calculated geometries around rhodium and phosphorus atoms of complex **2**; (c) calculated geometries around rhodium and phosphorus atoms of the transition state.

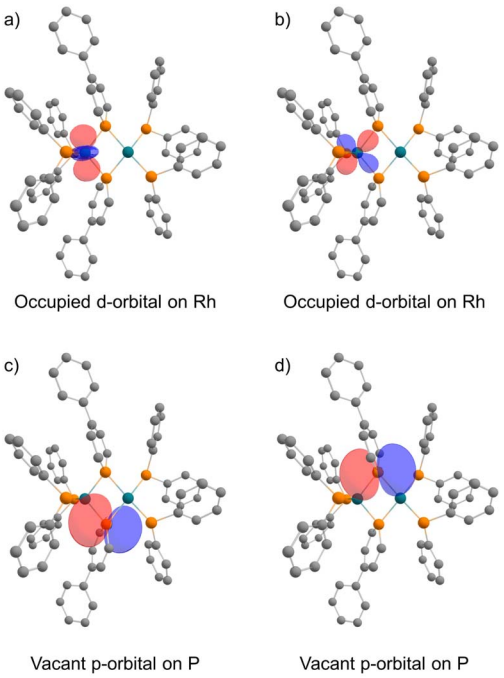

Fig. 8 Calculated NBOs of complex **2**: (a) and (b) occupied d-orbitals on the Rh atom; (c) and (d) vacant p-orbitals on P atoms (hydrogens and phenylene linkers are omitted for clarity).

occurred in the solution state. This result suggests that the unsymmetric structure of complex **2** is favourable compared with the symmetric structure. Therefore, the unsymmetric structure was considered for further discussion.

In the NBO analysis of complex **2** shown in Fig. 8 (calculated at the PBE0-D3/def2-TZVP//PBE0-D3/def2-SVP level), the vacant p-orbital of the phosphorus atom on phosphinine (Fig. 8a and b) and the occupied d-orbital of the Rh centre are overlapping each other (Fig. 8c and d). Second-order perturbation analysis suggested strong donation from the occupied d-orbital of the Rh centre to the vacant p-orbital of the P atoms on the phosphinine rings (see the ESI† for details). Interaction of these orbitals can be found in HOMO−40, HOMO−39, the HOMO, and the LUMO (Fig. 9). In HOMO−40 and HOMO−39, the bonding interaction of the square planar rhodium centre with the P atoms on the phosphinine rings also has some contribution. The existence of these orbitals accords with the electronic structure shown in Scheme 1, where the Rh(−I) centre donates d-electrons to the P atoms on the phosphinine rings and the lone pairs on the P atom are donated to the Rh(I) centre.

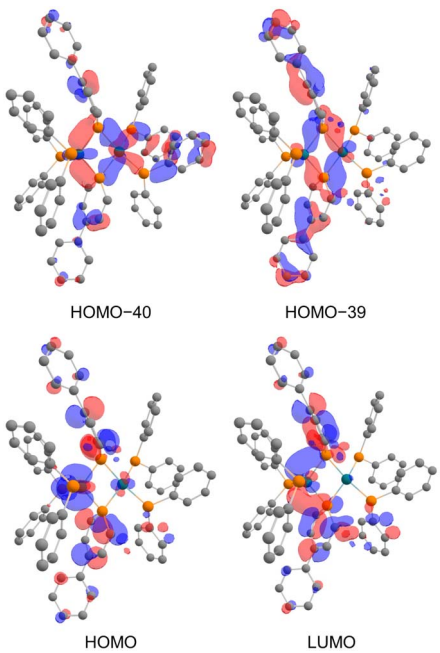

Fig. 9 Calculated molecular orbitals of complex **2** (hydrogens and phenylene linkers are omitted for clarity).

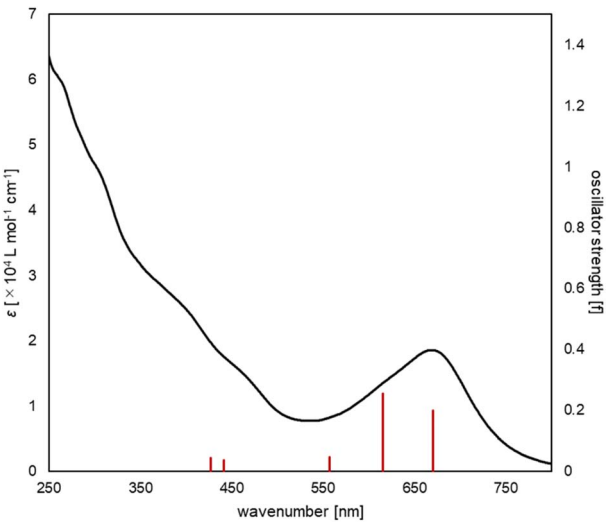

Fig. 10 UV/vis spectrum of complex **2** (black line, experimental, 1×10^{-5} M in THF), along with the oscillator strengths of complex **2** (red bars) obtained by the TD-DFT calculations.

The UV/vis absorption spectrum of complex **2** is shown in Fig. 10. The absorption spectrum of complex **2** (1×10^{-5} mol

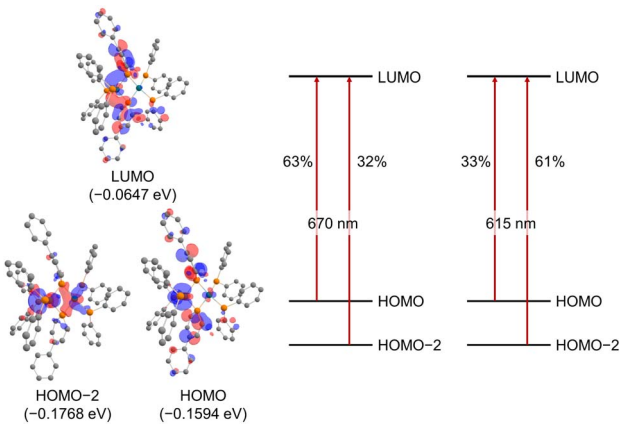

Fig. 11 Molecular orbitals of complex **2** (hydrogens and phenylene linkers are omitted for clarity) and major contributions to the absorption at 670 nm and 615 nm based on TD-DFT calculations (in THF).

L^{-1}) showed maximum absorption at 669 nm. TD-DFT calculations (calculated at the PBE0-D3/def2-TZVP//PBE0-D3/def2-SVP level) showed that the absorption of complex **2** at 669 nm can be assigned to the HOMO-to-LUMO and HOMO−2-to-LUMO transition ($\lambda_{calc} = 670$ nm ($f_{calc} = 0.1999$) and $\lambda_{calc} = 615$ nm ($f_{calc} = 0.2548$), Fig. 11). As shown in Fig. 11, this transition involves a d–d transition process (HOMO → LUMO), as well as an MLCT process (HOMO−2 → LUMO) like the previous reports on the photochemical properties of phosphinine metal complexes.[32,51–54]

Conclusions

This study presented the syntheses and structural analysis of dinuclear Rh(−I)/Rh(I) complex **2** bridged by phosphinine pincer ligands. The single-crystal X-ray crystallographic analysis showed an unsymmetric structure of complex **2** where the phosphinine ligands bridged two Rh centres in an unsymmetric mode. This suggests that complex **2** consists of a Rh(−I) centre and a Rh(I) centre. This electronic structure was supported by the DFT calculations, where back-donation from the tetrahedral Rh centre to the P atoms on the phosphinine rings was observed in the NBO analysis. As shown in this study, the phosphinine ligand gave rise to the unsymmetric electronic structure of a dinuclear metal complex. It will enable more precise control of the catalysis of dinuclear metal complexes.

Data availability

The data generated in this study are available in the main text or the ESI. Crystallographic data has been deposited at the joint Cambridge Crystallographic Data Centre (CCDC: 2260653 (**2**), 2260654 (**3**)). The NMR spectra and the cartesian coordinates of DFT optimized structure are provided in the ESI.†

Author contributions

K. M. and K. O. performed the synthesis and NMR experiments. K. M. and S. K. performed the crystallographic measurements. K. M. performed the DFT calculations. All authors analysed and discussed the results. K. M. prepared the manuscript with feedback from all authors. K. N. supervised the project.

Conflicts of interest

There are no conflicts to declare.

Acknowledgements

Part of this work was supported by "Advanced Research Infrastructure for Materials and Nanotechnology in Japan (ARIM)" of the Ministry of Education, Culture, Sports, Science and Technology (MEXT), (Grant Number JPMXP1222UT0194.). The computations were performed at the Research Center for Computational Science, Okazaki, Japan (Project: 23-IMS-C014). This work was supported by Grant-in-Aid for Challenging Research (Pioneering) JP22K19021, Noguchi institute research fund. K. M. is grateful to the Program for Leading Graduate Schools (MERIT-WINGS) and to the JSPS for a fellowship for young scientists.

Notes and references

1 E. K. van den Beuken and B. L. Feringa, *Tetrahedron*, 1998, **54**, 12985–13011.
2 J. I. van der Vlugt, *Eur. J. Inorg. Chem.*, 2012, **2012**, 363–375.
3 I. Bratko and M. Gómez, *Dalton Trans.*, 2013, **42**, 10664–10681.
4 J. A. Mata, F. Ekkehardt Hahn and E. Peris, *Chem. Sci.*, 2014, **5**, 1723–1732.
5 X. Huo, G. Li, X. Wang and W. Zhang, *Angew. Chem., Int. Ed.*, 2022, **61**, e202210086.
6 R. H. Crabtree, *The Organometallic Chemistry of the Transition Metals*, Wiley, 2014.
7 R. Colton and M. J. McCormick, *Coord. Chem. Rev.*, 1980, **31**, 1–52.
8 A. L. Sargent and M. B. Hall, *J. Am. Chem. Soc.*, 1989, **111**, 1563–1569.
9 A. A. Hock and O. S. Mills, *Acta Crystallogr.*, 1961, **14**, 139–148.
10 F. A. Cotton, B. A. Frenz and L. Kruczynski, *J. Am. Chem. Soc.*, 1973, **95**, 951–952.
11 F. A. Cotton and J. M. Troup, *J. Am. Chem. Soc.*, 1974, **96**, 1233–1234.
12 P. Macchi, L. Garlaschelli and A. Sironi, *J. Am. Chem. Soc.*, 2002, **124**, 14173–14184.
13 P. D. Burrow, A. J. Ashe III, D. J. Bellville and K. D. Jordan, *J. Am. Chem. Soc.*, 1982, **104**, 425–429.
14 M. Doux, A. Moores, N. Mézailles, L. Ricard, Y. Jean and P. L. Floch, *J. Organomet. Chem.*, 2005, **690**, 2407–2415.
15 C. Müller, L. E. E. Broeckx, I. de Krom and J. J. M. Weemers, *Eur. J. Inorg. Chem.*, 2013, **2013**, 187–202.
16 P. Le Floch and F. Mathey, *Coord. Chem. Rev.*, 1998, **178–180**, 771–791.
17 P. L. Floch, *Coord. Chem. Rev.*, 2006, **250**, 627–681.
18 N. T. Coles, A. Sofie Abels, J. Leitl, R. Wolf, H. Grützmacher and C. Müller, *Coord. Chem. Rev.*, 2021, **433**, 213729.
19 M. Doux, N. Mézailles, L. Ricard and P. Le Floch, *Eur. J. Inorg. Chem.*, 2003, **2003**, 3878–3894.
20 A. Campos-Carrasco, L. E. E. Broeckx, J. J. M. Weemers, E. A. Pidko, M. Lutz, A. M. Masdeu-Bultó, D. Vogt and C. Müller, *Chem.–Eur. J.*, 2011, **17**, 2510–2517.
21 J. Leitl, M. Marquardt, P. Coburger, D. J. Scott, V. Streitferdt, R. M. Gschwind, C. Müller and R. Wolf, *Angew. Chem., Int. Ed.*, 2019, **58**, 15407–15411.
22 P. Le Floch, D. Carmichael, L. Ricard and F. Mathey, *J. Am. Chem. Soc.*, 1993, **115**, 10665–10670.
23 K. Waschbüch, P. Le Floch, L. Ricard and F. Mathey, *Chem. Ber.*, 1997, **130**, 843–849.
24 N. Mézailles, P. Le Floch, K. Waschbüsch, L. Ricard, F. Mathey and C. P. Kubiak, *J. Organomet. Chem.*, 1997, **541**, 277–283.
25 R. J. Newland, J. M. Lynam and S. M. Mansell, *Chem. Commun.*, 2018, **54**, 5482–5485.

26 C. Tan, H. Tinnermann, V. Wee, S. Tan, S. Sung, Q. Wang and R. D. Young, *J. Organomet. Chem.*, 2023, **986**, 122617.
27 For a Mn_2 complex reported in the following reference, the phosphinine ligands are regarded as 3e donors, and the Mn_2 complex cannot be classified into the bridging modes shown in Fig. 1c: C. Elschenbroich, J. Six and K. Harms, *Chem. Commun.*, 2006, 3429–3431.
28 Y. Hou, Z. Li, Y. Li, P. Liu, C.-Y. Su, F. Puschmann and H. Grützmacher, *Chem. Sci.*, 2019, **10**, 3168–3180.
29 B. Schmid, L. M. Venanzi, T. Gerfin, V. Gramlich and F. Mathey, *Inorg. Chem.*, 1992, **31**, 5117–5122.
30 M. T. Reetz, E. Bohres, R. Goddard, M. C. Holthausen and W. Thiel, *Chem.–Eur. J.*, 1999, **5**, 2101–2108.
31 Y. Mao, K. M. H. Lim, Y. Li, R. Ganguly and F. Mathey, *Organometallics*, 2013, **32**, 3562–3565.
32 X. Chen, Z. Li, F. Yanan and H. Grützmacher, *Eur. J. Inorg. Chem.*, 2016, **2016**, 633–638.
33 M. H. Habicht, F. Wossidlo, T. Bens, E. A. Pidko and C. Müller, *Chem.–Eur. J.*, 2018, **24**, 944–952.
34 J. Leitl, P. Coburger, D. J. Scott, C. G. P. Ziegler, G. Hierlmeier, R. Wolf, N. P. van Leest, B. de Bruin, G. Hörner and C. Müller, *Inorg. Chem.*, 2020, **59**, 9951–9961.
35 M. J. Bakker, F. W. Vergeer, F. Hartl, K. Goubitz, J. Fraanje, P. Rosa and P. Le Floch, *Eur. J. Inorg. Chem.*, 2000, **2000**, 843–845.
36 M. J. Bakker, F. W. Vergeer, F. Hartl, P. Rosa, L. Ricard, P. Le Floch and M. J. Calhorda, *Chem.–Eur. J.*, 2002, **8**, 1741–1752.
37 S. Giese, K. Klimov, A. Mikeházi, Z. Kelemen, D. S. Frost, S. Steinhauer, P. Müller, L. Nyulászi and C. Müller, *Angew. Chem., Int. Ed.*, 2021, **60**, 3581–3586.
38 F. Nief, C. Charrier, F. Mathey and M. Simalty, *J. Organomet. Chem.*, 1980, **187**, 277–285.
39 H. Lehmkuhl, R. Paul and R. Mynott, *Liebigs Ann. Chem.*, 1981, **1981**, 1139–1146.
40 E. Yue, A. Petrov, D. S. Frost, L. Dettling, L. Conrad, F. Wossidlo, N. T. Coles, M. Weber and C. Müller, *Chem. Commun.*, 2022, **58**, 6184–6187.
41 P. Rosa, L. Ricard, F. Mathey and P. Le Floch, *Organometallics*, 2000, **19**, 5247–5250.
42 J. Abbenseth and J. M. Goicoechea, *Chem. Sci.*, 2020, **11**, 9728–9740.
43 S. J. Hwang, A. Tanushi and A. T. Radosevich, *J. Am. Chem. Soc.*, 2020, **142**, 21285–21291.
44 M. J. Drance, A. Tanushi and A. T. Radosevich, *J. Am. Chem. Soc.*, 2022, **144**, 20243–20248.
45 K. Masada, S. Kusumoto and K. Nozaki, *Angew. Chem., Int. Ed.*, 2022, **61**, e202117096.
46 K. Masada, S. Kusumoto and K. Nozaki, *Organometallics*, 2023, **42**, 971–981.
47 L. Yang, D. R. Powell and R. P. Houser, *Dalton Trans.*, 2007, 955–964.
48 M. Carvalho, L. F. Wieserman and D. M. Hercules, *Appl. Spectrosc.*, 1982, **36**, 290–296.
49 J. P. Contour, G. Mouvier, M. Hoogewys and C. Leclere, *J. Catal.*, 1977, **48**, 217–228.
50 H. Kameo, Y. Hashimoto and H. Nakazawa, *Organometallics*, 2012, **31**, 3155–3162.
51 J. Moussa, T. Cheminel, G. R. Freeman, L.-M. Chamoreau, J. A. G. Williams and H. Amouri, *Dalton Trans.*, 2014, **43**, 8162–8165.
52 J. Moussa, L. M. Chamoreau and H. Amouri, *RSC Adv.*, 2014, **4**, 11539–11542.
53 P. Roesch, J. Nitsch, M. Lutz, J. Wiecko, A. Steffen and C. Müller, *Inorg. Chem.*, 2014, **53**, 9855–9859.
54 Y. Li, Z. Li, Y. Hou, Y.-N. Fan and C.-Y. Su, *Inorg. Chem.*, 2018, **57**, 13235–13245.